Numerical Simulation of Flow over Backward-Facing Step Using Parallel Multi-Block Compact Method

V. Esfahanian, F. Torabi, A. Khajavi Rad and H. Babaee

Mechanical Engineering Department, University of Tehran, Tehran, Iran

Email*:* *evahid@ut.ac.ir*

ABSTRACT

In this study the accurate location of separation and reattachment points in the flow over backward-facing step have been determined for 100<Re<800. Two-dimensional steady incompressible Navier-Stokes equations have been solved using stream function-vorticity formulation, along with fourth-order upwind compact finite difference method. Considering high computational cost of the compact method, a parallel multi-block algorithm has been implemented to reduce the execution time. According to this scheme the main domain is decomposed into several equal size sub-blocks which each will be solved by different processors independently. Each node will receive its boundary values from adjacent processors during iteration by introducing the concept of "ghost points". Parallelizing has been achieved through a Beowulf system which contains a cluster of PCs with distributed memory. MPI library has been used for passing messages between various nodes. In order to verify the obtained results, the loci of separation and reattachment points have been compared with other experimental and numerical results. Finally, speed up and performance of parallel algorithm have been examined.

NOMENCLATURE

ψ Stream function in physical domain

Ψ Stream function in computational domain

$\Psi F\xi$ First derivative of stream function in ξ-direction

$\Psi F\eta$ First derivative of stream function in η-direction

$\Psi S\xi$ Second derivative of stream function in ξ-direction

$\Psi S\eta$ Second derivative of stream function in η- direction

ω Vorticity in physical domain

Z Vorticity in computational domain

$ZF\xi$ First derivative of vorticity in ξ-direction

$ZF\eta$ First derivative of vorticity in η-direction

$ZS\xi$ Second derivative of vorticity in ξ-direction

$ZS\eta$ Second derivative of vorticity in η-direction

ξFX ξ_x, The *x*-metric of coordinate ξ

ξSX ξ_{xx}, The first derivative of *x*-metric of coordinate ξ

ηFY η_y, The *y*-metric of coordinate η

ηSY η_{yy}, The first derivative of *y*-metric of coordinate η

u Velocity component in *x*-direction

v Velocity component in *y*-direction

m Index of grid points in *x*-direction

n Index of grid points in *y*-direction

1. INTRODUCTION

The phenomena of flow separation and reattachment as fluid encounter with a sudden change in geometry have great importance in many engineering equipment and aerodynamic devices. Comprehensive attempts have been made in order to examine the accurate behavior of flows with separated regions (Durst & Whitelaw, 1971; Gosman & Pun, 1974; Kumar & Yanjnik, 1980; Adams & Johnston, 1988). Among these, the problem of steady viscous incompressible flow over a two dimensional backward-facing step has been the main target of many researchers. Numerous experimental (Denham & Patrick, 1974; Armaly & Durst [2], 1983) and numerical techniques (Osswald & Ghia, 1983; Kim & Moin [5], 1985; Gartling [3], 1990; Kaiktsis [4], 1991; Williams & Bakers, 1997; Barkley & Henderson [4], 2002) have been developed in this field. The reason for such a particular attention is that although owing a simple geometry, it can capture complex flow features associated with separation and reattachment. Therefore, the flow over backward-facing step has become a well-known benchmark to validate the accuracy of any numerical schemes by computing the accurat location of the separation and reattachment points. On of the main difficulties while applying various numerical schemes is the highly dependence of the recirculation length with respect to the numerical mesh, causing what is known as false diffusion.

In this study, in order to determine the accurate location of separation and reattachment points a fourth-order upwind compact finite difference method has been implemented. The fourth order accuracy of this method made it more efficient in the term of the grid resolution and as a result preventing false diffusion. Considering high computational cost of the compact method a parallel multi-block algorithm is implemented to reduce the execution time. In this scheme the computational domain is decomposed into several equal size sub-blocks which each one will be solved by different processors independently.

2. PROBLEM DEFINITION

The problem geometry is considered as was addressed by Gartling [2] which consists of the standard step with expansion ratio 1:2 and excluding the upstream channel. In order to reach a fully developed condition, the step length is settled according to Reynolds number. The boundary conditions include no-slip velocity condition for all solid walls and a fully developed condition at inlet and exit. The velocity profile at inlet assumed to be parabolic with average velocity of 1 m/sec (Fig. 1). The Reynolds number is defined by Re=$u_{ave}H/\nu$. To capture the strong gradients adjacent to solid walls and the formation of the recirculation regions, a nonuniform mesh with clustering near the walls in vertical direction and near the step in horizontal direction is used (Fig. 2).

3. GOVERNING EQUATIONS

For steady viscous incompressible flow over a two-dimensional backward-facing step, stream function and vorticity transport equations in nondimensional form are as follow:

1) Stream function equation:

$$\frac{\partial^2\psi}{\partial x^2}+\frac{\partial^2\psi}{\partial y^2}=-\omega \qquad (1)$$

Where ψ and ω denote for stream function and vorticity, respectively.

2) Vorticity transport equation:

$$u\frac{\partial\omega}{\partial x}+v\frac{\partial\omega}{\partial y}=\frac{1}{\text{Re}}\left(\frac{\partial^2\omega}{\partial x^2}+\frac{\partial^2\omega}{\partial y^2}\right) \qquad (2)$$

As it was mentioned in section 2, a nonuniform grid with clustering in both vertical and horizontal directions is applied. Writing equations (1) and (2) in the computational domain, one can obtain:

$$\xi_x^2\frac{\partial^2\psi}{\partial\xi^2}+\xi_{xx}\frac{\partial\psi}{\partial\xi}+\eta_y^2\frac{\partial^2\psi}{\partial\eta^2}+\eta_{yy}\frac{\partial\psi}{\partial\eta}=-\omega \qquad (3)$$

$$u\xi_x\frac{\partial\omega}{\partial\xi}+v\eta_y\frac{\partial\omega}{\partial y}= \qquad (4)$$

$$\frac{1}{\text{Re}}\left(\xi_x^2\frac{\partial^2\omega}{\partial\xi^2}+\xi_{xx}\frac{\partial\omega}{\partial\xi}+\eta_y^2\frac{\partial^2\omega}{\partial\eta^2}+\eta_{yy}\frac{\partial\omega}{\partial\eta}\right)$$

which ξ and η are the equal-spaced grid points in the rectangular computational domain.

In order to solve this system of nonlinear equations, the 4th-order upwind compact finite-difference relations are implemented. The tridiagonal nature of the involved matrices is maintained by applying ADI method. Applying the above method for stream function in *x*- direction, the following relations are obtained:

$$\frac{1}{\Delta t}\Psi^*_{m,n}-\xi FX^2_{m,n}\Psi S\xi^*_{m,n}-\xi SX_{m,n}\Psi F\xi^*_{m,n}=$$

$$\omega^n_{m,n}+\frac{1}{\Delta t}\Psi_{m,n}+\eta FY^2_{m,n}\Psi S\eta^n_{m,n}+\eta SY_{m,n}\Psi F\eta^n_{m,n}$$

$$\frac{1}{6}\Psi F\xi^*_{m-1,n}+\frac{2}{3}\Psi F\xi^*_{m,n}+ \qquad (5)$$

$$\frac{1}{6}\Psi F\xi^*_{m+1,n}-\frac{1}{2}(\Psi^*_{m+1,n}-\Psi^*_{m-1,n})=0$$

$$\frac{1}{12}\Psi S\xi^*_{m-1,n}+\frac{5}{6}\Psi S\xi^*_{m,n}+\frac{1}{12}\Psi S\xi^*_{m+1,n}$$

$$-(\Psi^*_{m-1,n}-2\Psi^*_{m,n}+\Psi^*_{m+1,n})=0$$

And for ψ in the *y*-direction we can write:

$$\frac{1}{\Delta t}\Psi^{n+1}_{m,n}-\eta FY^2_{m,n}\Psi S\eta^{n+1}_{m,n}-\eta SY_{m,n}\Psi F\eta^{n+1}_{m,n}=$$

$$\omega^n_{m,n}+\frac{1}{\Delta t}\Psi^n_{m,n}+\eta FY^2_{m,n}\Psi S\eta^n_{m,n}+\eta SY_{m,n}\Psi F\eta^n_{m,n}$$

$$\frac{1}{6}\Psi F\eta^{n+1}_{m,n-1}+\frac{2}{3}\Psi F\eta^{n+1}_{m,n}+\frac{1}{6}\Psi F\eta^{n+1}_{m,n+1} \qquad (6)$$

$$-\frac{1}{2}(\Psi^{n+1}_{m,n+1}-\Psi^{n+1}_{m,n-1})=0$$

$$\frac{1}{12}\Psi S\eta^{n+1}_{m,n-1}+\frac{5}{6}\Psi S\eta^{n+1}_{m,n}+\frac{1}{12}\Psi S\eta^{n+1}_{m,n+1}$$

$$-(\Psi^{n+1}_{m,n-1}-2\Psi^{n+1}_{m,n}+\Psi^{n+1}_{m,n+1})=0$$

The derived equations for ω in the *x*-direction are therefore:

$$\frac{1}{\Delta t}Z^*_{m,n}+u.\xi FX_{m,n}ZF\xi^*_{m,n}$$

$$-\frac{1}{\text{Re}}(\xi FX^2_{m,n}ZS\xi^*_{m,n}+\xi SX_{m,n}ZF\xi^*_{m,n})= \qquad (7)$$

$$\frac{1}{\Delta t}Z^n_{m,n}-v.\eta FY_{m,n}ZF\eta^n_{m,n}$$

$$+\frac{1}{\text{Re}}(\eta FY^2_{m,n}ZS\eta^n_{m,n}+\eta SY_{m,n}ZF\eta^n_{m,n})$$

If $u_{m,n}>0$ backward compact finite-differencing yields:

$$\frac{5}{12}ZF\xi^{*}_{m-1,n}+\frac{8}{12}ZF\xi^{*}_{m,n}-\frac{1}{12}ZF\xi^{*}_{m+1,n}$$
$$-(Z^{*}_{m,n}-Z^{*}_{m-1,n})=0$$

If $u_{m,n}<0$ forward compact finite-differencing gives:

$$\frac{1}{12}ZF\xi^{*}_{m-1,n}+\frac{8}{12}ZF\xi^{*}_{m,n}-\frac{5}{12}ZF\xi^{*}_{m+1,n}$$
$$-(Z^{*}_{m+1,n}-Z^{*}_{m,n})=0$$
$$\frac{1}{12}ZS\xi^{*}_{m-1,n}+\frac{5}{6}ZS\xi^{*}_{m,n}+\frac{1}{12}ZS\xi^{*}_{m+1,n}$$
$$-(Z^{*}_{m-1,n}-2Z^{*}_{m,n}+Z^{*}_{m+1,n})=0$$

The derived equations for ω in the y-direction are:

$$\frac{1}{\Delta t}Z^{n+1}_{m,n}+v.\eta FY_{m,n}ZF\eta^{n+1}_{m,n}$$
$$-\frac{1}{\mathrm{Re}}(\eta FY^{2}_{m,n}ZS\eta^{n+1}_{m,n}+\eta SY_{m,n}ZF\eta^{n+1}_{m,n})= \qquad (8)$$
$$\frac{1}{\Delta t}Z^{n}_{m,n}-u.\xi FX_{m,n}ZF\xi^{n}_{m,n}$$
$$+\frac{1}{\mathrm{Re}}(\xi FX^{2}_{m,n}ZS\xi^{n}_{m,n}+\xi SX_{m,n}ZF\xi^{n}_{m,n})$$

If $v_{m,n}>0$, then a backward compact finite-differencing are used:

$$\frac{5}{12}ZF\eta^{n+1}_{m,n-1}+\frac{8}{12}ZF\eta^{n+1}_{m,n}-\frac{1}{12}ZF\eta^{n+1}_{m,n+1}$$
$$-(Z^{n+1}_{m,n}-Z^{n+1}_{m,n-1})=0$$

For $v_{m,n}<0$, a forward compact finite-differencing are implemented as:

$$\frac{1}{12}ZF\eta^{n+1}_{m,n-1}+\frac{8}{12}ZF\eta^{n+1}_{m,n}-\frac{5}{12}ZF\eta^{n+1}_{m,n+1}$$
$$-(Z^{n+1}_{m,n+1}-Z^{n+1}_{m,n})=0$$
$$\frac{1}{12}ZS\eta^{n+1}_{m,n-1}+\frac{5}{6}ZS\eta^{n+1}_{m,n}+\frac{1}{12}ZS\eta^{n+1}_{m,n+1}$$
$$-(Z^{n+1}_{m,n-1}-2Z^{n+1}_{m,n}+Z^{n+1}_{m,n+1})=0$$

Due to the fact that the 4^{th}-order accuracy of the compact method is highly dependent on the way the metric derivatives are obtained; these parameters are calculated numerically using 4^{th}-order compact finite difference relations.

4. PARALLEL ALGORITHM

In this study, the main objective for parallelization is to minimize the execution time; consequently, the following factors must be taken into account:

1. Increasing the fraction of the program that can be parallelized.
2. Balancing the workload of parallel processes.
3. Minimizing the time spent for communication.

In order to balance the working load among the processors, in the case of a homogeneous network of processors, the computational domain is decomposed into a number of equal size sub-blocks. The sub-domains are solved by different nodes concurrently and during the communication time each processor receives its boundary values from its neighbors by introducing the concept of “ghost points”. Domain decomposition can be achieved in various ways (e.g. row wise, column wise or checker board block decomposition). Applying the scalability theorem and isoefficiency relation, it can be shown that the most efficient algorithm in decomposing the main domain is the checker board method [7]. For a fixed number of processors there are several ways in choosing the shape of sub-blocks in checker board decomposition method. But the most efficient way is to distribute the main domain such that the rectangular block for each processor becomes as close to square as possible. This fact is based on the following observation: since for a fixed area (i.e. fixed number of the total grid points) the communication time is proportional to the perimeter of the sub-block (i.e. number of the boundary grids), the communication time is minimized for a square shaped sub-block for each processor.

5. NUMERICAL RESULTS

In order to parallelize the code the main domain is decomposed into 10 equal size sub-blocks which are solved by different processors separately (Fig. 3). Separation and reattachment points have been located (Table 1) and compared with other experimental and numerical methods (Fig. 4). As it can be seen for Re<400, a range in which the two-dimensionality of the flow maintains, the compact method shows satisfactory agreement with experiment. With the formation of the second recirculation zone for Re>400, the flow become three dimensional and the results deviate from those of the experiment but still show better agreement with those of other two dimensional numerical schemes.

The flow over the backward-facing step for Re=800 has been considered in more detail. In order to achieve the fully developed condition at the flow outlet, the channel length is considered to be 60 step heights. The velocity vectors and pressure contours are shown in figures 5 and 6, respectively. To find the minimum resolution required for mesh-independent results, the flow has been simulated versus four different mesh configurations (Fig. 7). Results show that due to the fourth-order accuracy of the compact method, the results are less dependent on mesh sizes compared with the other applied methods. The location of separation and reattachment points for Re=800 are compared with [3] and [4] (Table 2) and show good agreement with them.

The accuracy order of the compact method is determined experimentally by sketching the point wise error versus uniformly refined grids for a fixed point. The error is defined as the absolute difference between the stream function for each mesh configuration and that of the most refined one. The plot has been sketched for four different mesh sizes at Re=100 for a fixed point located at x=3.20 and y=0.50. Figure 8 shows that the diagram is approximately a straight line which has a slope equal to 3.61. This value provides us with the actual accuracy order of the compact scheme compared with the theoretical one.

In order to show the performance of the parallel algorithm, speed up and efficiency diagrams are sketched for three different mesh sizes at Re=100 (Fig. 9, 10). As it is shown with increasing the number of processors, execution time decreases considerably which shows the effectiveness of applying parallel processing in time consuming problems. Figure 8 shows that for any fixed the number of processors, the speed up is usually an increasing function of problem size, which is called Amdahl effect. As it can be seen from Figure 9, parallel algorithm efficiency decreases as the number of processors are increased. This fact is due to the lack of enough scalability of compact method. Thus, in order to maintain the same level of efficiency as the number of processors increases, the problem size must be increased accordingly.

6. CONCLUSIONS

A fourth-order upwind compact finite difference method has been presented for simulating flow over a two-dimensional backward-facing step for 100<Re<800. Considering the high computational cost of the compact method, a parallel multi-block scheme was implemented. Parallelizing has been achieved through a Beowulf system which contains a cluster of PCs in order to reduce the execution time.

Separation and reattachment points were located and compared with other experimental and numerical models. Results shows good agreement with experiment in the region where the two dimensional numerical models remain valid. But for Reynolds numbers in the excess of 400, there is a considerable deviation from the experiment which is due to flow three-dimensionality effects.

AKNOWLEDGEMENTS

The authors would like to thank ADSRC for computer resources and also the support of the Vehicle, Fuel and Environment Research Institute (VFERI) and University of Tehran. Authors would also like to acknowledge Khosro Ashrafi and Hossein Mahmoodi for their valuable comments on this paper.

REFERENCES

[1] V. Esfahanian, M. Tabesh, H. Sayevand, “Numerical Simulation of Flow in a Lid-Driven Cavity Using Compact Method,” The 7th International Conference of Mechanical Engineering, 1993.

[2] F. Armaly, F. Durst, J. C. F. Pereire and B. Schonung, “Experimental and Theoretical Investigation of Backward Facing Step Flow,” Journal of Fluid Mechanics, Vol 127, PP. 437-496, 1983.

[3] K. Gartling, “A Test Problem for Outflow Boundary Conditions - Flow over Backward Facing Step,” International Journal for Numerical Methods in Fluids, Vol 11, PP. 953-967, 1990.

[4] D. Barkley, M. Gabriela, M. Gomes and R. Henderson, “Three Dimensional Instability in Flow Over a Backward-Facing Step,” Journal of Fluid Mechanics, Vol 127, PP. 437-496, 2002.

[4] L. Kaiktsis, G. E. Karniadakis and S. A. Orszag, “Onset of Three-Dimensionality, Equilibria, and Early Transition in Flow over a Backward Facing Step,” Journal of Fluid Mechanics, Vol. 231, PP. 501-528, 1991.

[5] J. Kim, P. Moin, “Application of a Fractional-Step Method to Incompressible Navier-Stokes Equations,” Journal of Computational Physics, Vol. 59, PP. 308-314, 1985.

[6] G. A. Osswald, K. N. Ghia and U. Ghia, “Study of Incompressible Separated Flow Using Implicit Time-dependent Technique,” AIAA Sixth CFD Conference, Danvers, MA, PP. 686-692, 1983.

[7] J. Sohn, “Evolution of FIDAP on some classical laminar and turbulent benchmarks,” Int. J. Numer. Methods Fluids, Vol. 8, pp. 1469-1490, 1988.

[8] M. J. Quinn, *Parallel Programming in C with MPI and Open MP*, McGraw Hill, Singapore, 2003.

[9] “Introduction to MPI,” created by the PACS Training Group, Board of the university of Illinois, 2001.

[10] P. Parikh, “Application of a Scalable, Parallel, Unstructured-Grid-Based Navier-Stokes Solver,” 15th AIAA Computational Fluid Dynamics Conference, California, 2001.

Table 1: Location of separation and reattachment points at *Re*=800.

Re	Lower reattachment point	Upper separation point	Upper reattachment point
100	1.27	–	–
200	2.35	–	–
300	3.23	–	–
400	4.09	3.76	4.97
500	4.69	3.91	6.54
600	5.14	4.17	7.90
700	5.54	4.39	9.11
800	5.90	4.64	10.28

Table 2: Comparison of separation and Reattachment points at *Re*=800.

Case Study	Lower reattachment point	Upper separation point	Upper reattachment point
Sohn (1988)	5.8	4.55	9.25
Gartling (1990)	6.1	4.85	10.5
Barkley (2002)	5.95	4.75	10.3
Proposed Method	5.90	4.64	10.28

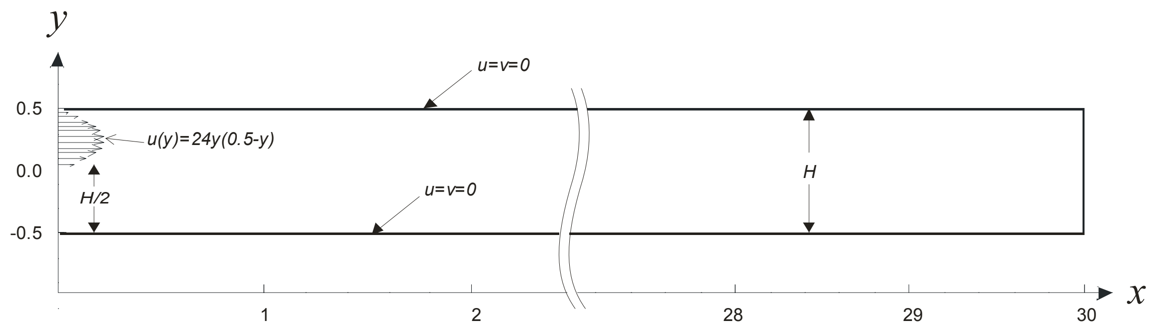

Figure 1: Back-ward facing step geometry and applied boundary conditions.

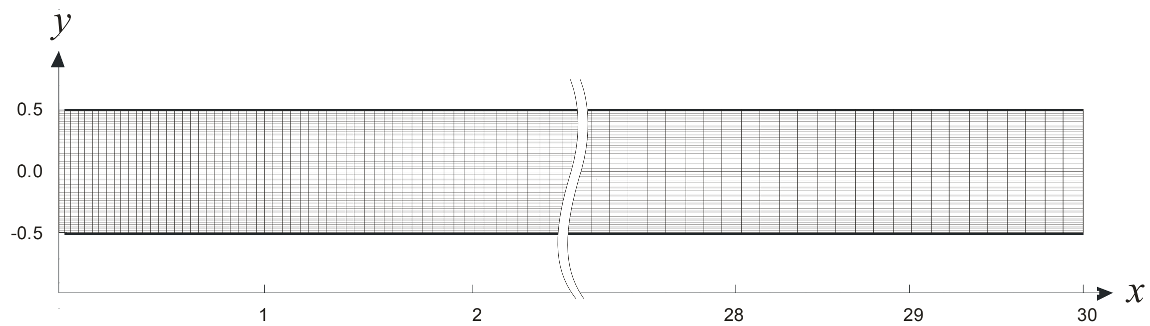

Figure 2: The computational mesh with 300×50 grid points.

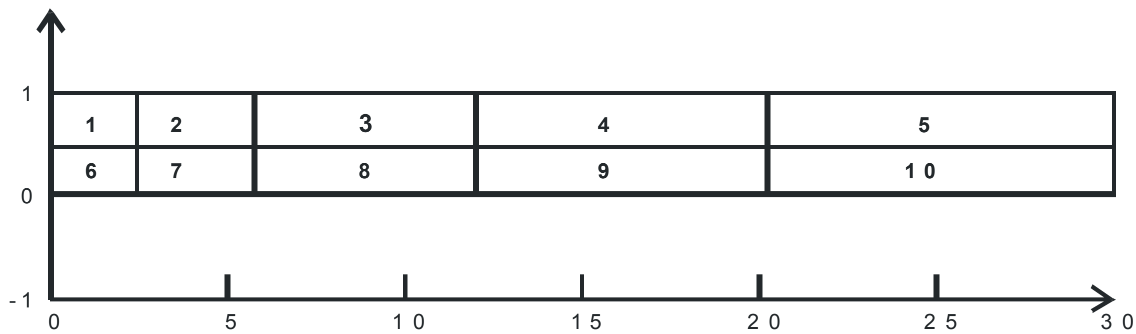

Figure 3: Domain decomposition between 10 processors.

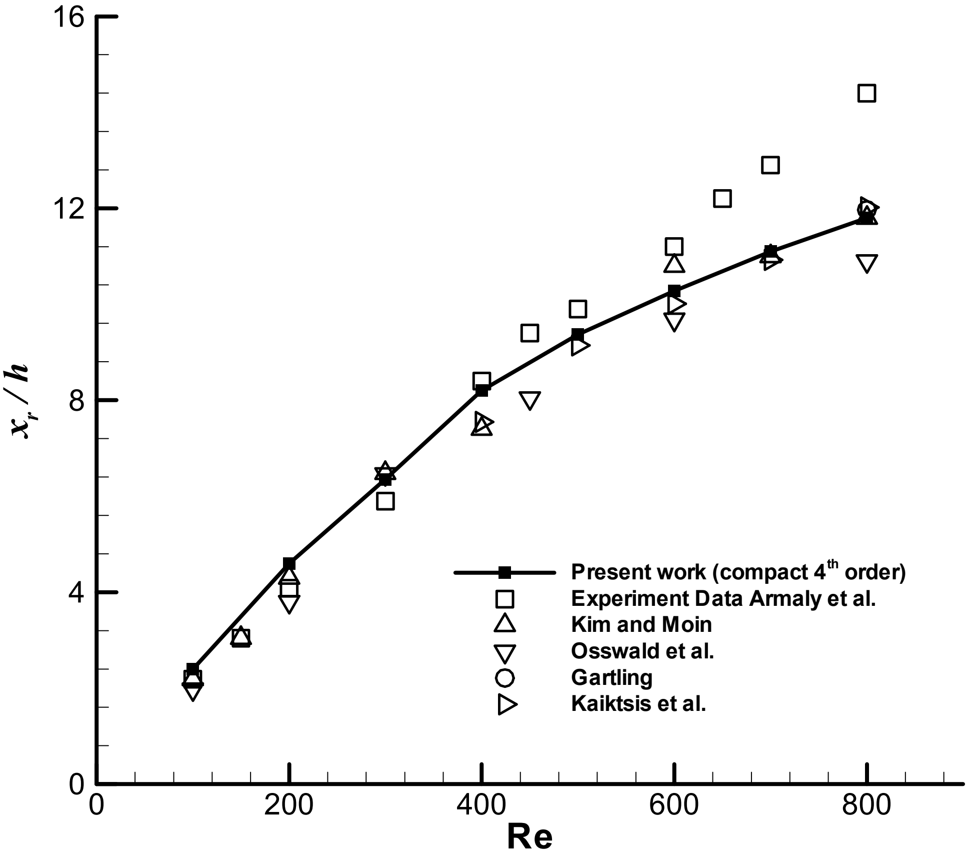

Figure 4: Comparison of experimental and theoretical results for reattachment length.

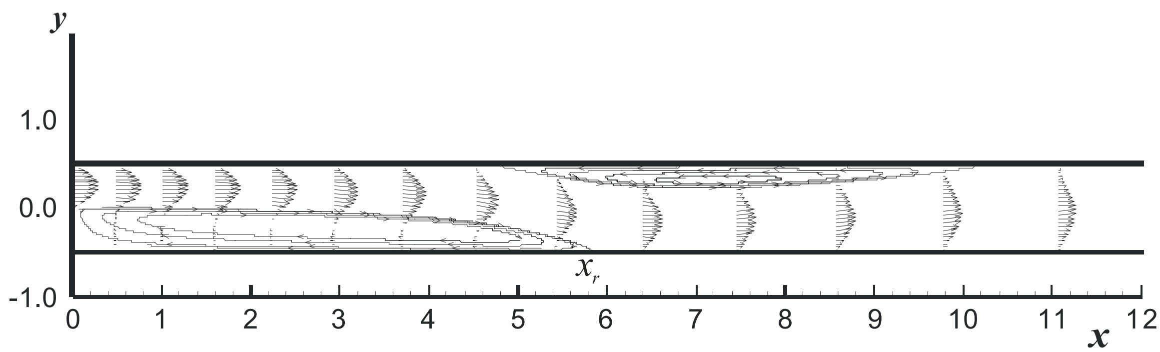

Figure 5: Velocity vectors at Re=800.

Figure 6: Pressure contours at Re=800.

Figure 7: Vorticity at lower wall versus different mesh configurations.

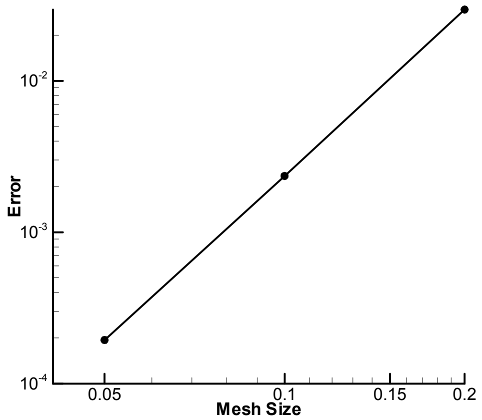

Figure 8: Error analysis for the fourth-order compact scheme.

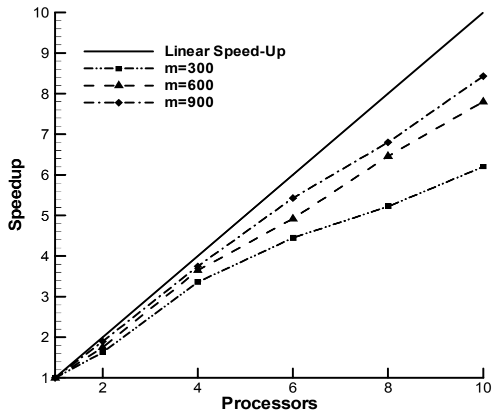

Figure 9: Speedup vs. number of CPUs.

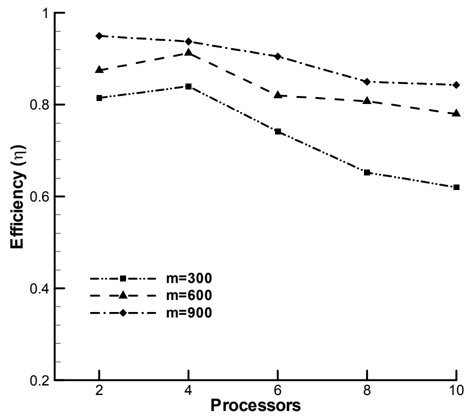

Figure 10: Efficiency vs. number of CPUs.